MULTI-SCALE INTERNAL GEOMETRY ANALYSIS AND MECHANICAL MODELING OF RANDOMLY ORIENTED STRANDS

Yi Wan [1] * and Jun Takahashi [1]

[1] Department of Systems Innovation, the University of Tokyo, Japan
* Corresponding author: wan-yi@cfrtp.t.u-tokyo.ac.jp

Keywords: CFRTP, ROS, internal geometry, modeling

ABSTRACT

Adequate characterization of the internal geometry of randomly oriented strands (ROS) for prediction of their properties requires acquisition and analysis of vast amount of data. In the present work, one kind of ROS fabricated with carbon fiber reinforced thermoplastics (CFRTP), so called ultra-thin chopped carbon fiber tape reinforced thermoplastics (UT-CTT), were introduced for the research of multi-scale internal geometry analysis and mechanical modeling methods. Two different methods were proposed to measure and quantify the internal geometry of UT-CTT using X-ray micro-CT. One method based on image binarization and another one based on structure tensor. The two-scale fiber orientation distributions (orientation of the tapes and of the fibers inside the tapes), tape morphology, 3D structure and orientation misalignment were characterized. After the detailed micro-structure information of UT-CTT collected through the internal geometry study, one-step Mori-Tanaka model and mean-filed homogenization based equivalent laminate model were applied for the simulation of mechanical properties. The simulated properties were also compared with the experimental data.

The results indicate that the applied X-ray micro-CT methods can provide detailed information like primary orientation directions, tape waviness, and splitting of the internal geometry of UT-CTT. And the two mechanical models show their advantages and disadvantage on prediction the modulus and strength of UT-CTT. In comparison with the traditional discontinuous CFRTP sheet molded compound (SMC), the UT-CTT exhibited superiorities in terms of computer aided engineering (CAE) capability and internal geometry regularity.

1 INTRODUCTION

Carbon fiber reinforced thermoplastics (CFRTP) are increasingly used as replacement materials for traditional carbon fiber reinforced thermosets (CFRTS), not only because they provide superior recyclability, but also because they can be produced by rapid cycle molding processing without solvent. Using thin layers in laminate composites can improve mechanical performance, as verified by Sihn et al. [1], Yokozeki et al. [2] and Amacher et al. [3] among others. Randomly oriented discontinuous CFRTP can bring about high-quality complex geometry molding and promote the usage of recycled materials. Randomly oriented strands (ROS), as a representative randomly-oriented discontinuous fiber reinforced composite with a high fiber volume content, show a combination of favorable complex molding capability and high mechanical performance; new research is being rapidly carried out in this field [4-6]. Therefore, ROS fabricated with CFRTP thin ply pre-impregnated strands are considered to be advantageous composites and regarded as potential substitutes for metallic materials in various mass-produced applications [7].

To ensure the reliability and safety of ROS in industrial applications, the material's structure and properties must be comprehensively analyzed. X-ray micro-computed tomography (micro-CT) is a powerful non-destructive method for the characterization and visualization of the internal geometry in composite materials. ROS generally have complex internal geometry due to strands distribution during fabricating, and X-ray micro-CT is considered to be an efficient method to provide higher accuracy in the characterization of fiber orientation distribution (FOD), fiber length distribution (FLD) and multi-scale geometry quantification. The X-ray micro-CT researches of fiber reinforced composite materials

were mainly concentrated on the injection molding compound [8-13], laminates [14-16] and woven fabric composites [17-20]. The distributions of fiber morphologies were studied by Alemdar et al. [8]. Local average orientation distribution and visualized 3D orientation modeling of GF/PA6 injection materials were investigated by Bernasconi et al. [9] using the Mean Intercept Length (MIL) technique. Fiber orientation and effect of injection flow on injecting molded glass fiber reinforced nylon (GF/PA6) and carbon fiber reinforced polypropylene (CF/PP) were analyzed respectively [12, 13]. The orientation distribution together with local volume fraction of CF/Aluminum and CF/epoxy unidirectional laminates were investigated through 3D micro-CT method [14]. 2D laminated preform and random felt carbon-carbon composites were fabricated, and studied by Dietrich et al. focusing on distribution of the fibers, porosity and other internal geometries [15]. The porosity of CF/epoxy laminates were also studied and the X-ray micro-CT aided mechanical simulations were conducted by Tserpes et al. [16]. The internal geometries of carbon woven fabric [17] and woven textile CF/epoxy composites [18] were analyzed using a structural tensor based micro-CT method. The combination of the reconstructed 3D model of both short fiber composites and textile composites with the FE mesh generation and numerical analysis have been reported [11, 19]. However, none of the referenced studies considered the X-ray micro-CT analysis of ROS composites.

The mechanical properties of discontinuous CFRTP have been studied previously through different approaches for accurate and effective estimation. Fu et al. calculated the tensile modulus and strength of CFRTP in different fiber aspect ratios and orientations based on the modified rule of mixtures [21, 22]. Piggott et al. verified the accuracy of the shear-lag model for the simulation of the mechanical performance of short fiber reinforced plastics [23]. An accurate multi-scale FE (finite element) model has been established by Hashimoto et al. for simulating the tensile strength of discontinuous carbon fiber/polypropylene composites with fiber orientation distribution [24]. Further, a comparison between the analytical and numerical homogenization methods was conducted by using a complex multi-scale FE model, as well as one step Mori–Tanaka model, two-step Self-Consistent/Voigt model, and Lielens (Li)/Voigt model [25]. Recently, Pimenta and co-workers simulated the tensile properties of prepreg-based discontinuous composites with a shear-lag-based equivalent laminate method [26]. Thus far, the combination of the Mori–Tanaka type model [27] with the Eshelby's equivalent inclusion method [28] presents one of the most efficient and accurate approaches for the prediction of composite stiffness. However, the previous researches indicated the limitation in the volume fraction and orientation distribution of the inclusions of this method [25, 29-31], and the reason for this limitation remains unclear.

In present study, the internal geometries and mechanical properties of UT-CTT with different tape length are characterized, two X-ray micro-CT methods and two modeling methods are applied in this research. The multi-scale internal geometries are quantified and visualized, the tensile properties are evaluated and compared with experimental results.

2 MATERIALS AND METHODS

2.1 Materials

In this study, the UT-CTT were fabricated by randomly oriented ultra-thin unidirectional pre-impregnated sheets (44 μm thickness in average). The ultra-thin sheets were manufactured by spread carbon fiber tow (TR 50S, Mitsubishi Rayon Co., LTD.) and Polyamid-6 (PA6, DIAMIRON™ C, Mitsubishi Plastics, Inc.). The average fiber volume fraction (V_f) of the sheets is 55% and the V_f of UT-CTT after molding were calculated through the ash test. The ash test is used to determine the actual V_f of composites by measuring the sample volume V using a densitometer and the weight of CF M_{CF} by burning the resin off. The pre-impregnated sheets were provided by the Industrial Technology Center of Fukui Prefecture in Japan. The sheets were cut into three different tape sizes in present study. Tape length 12 mm, 18 mm, 24 mm, and 30 mm were selected, and the tape width was fixed to 5 mm. To manufacture the UT-CTT, the discontinuous tapes are dispersed by wet-type paper making process. The tapes are randomly distributed in water and the tape sheets are stacked to make the UT-CTT plate by heating-and-cooling compression molding (Fig. 1). The molding pressure was 5 MPa, which is the recommended molding pressure based on previous researches [32]. The molded plates are 2 mm in

thickness. This material shows good transverse isotropy, and because the fibers were impregnated before molding, the UT-CTT can be molded under low molding pressure, which is a big advantage for the mass-production applications. Additionally, since the V_f of this material can reach over 50%, this material is presumed to be applicable to the critical components of vehicles.

After the UT-CTT plates are made, the specimens for X-ray measurement and tensile tests are prepared. To ensure the sufficient resolution of the X-ray images and provide reliable information on the internal geometry and fibers, the specimens must be cut in relatively small size. After each edge of the plates was cut off by 15 mm to eliminate the molding edge effect, the X-ray specimens with a size of 2×2×30 mm (thickness × width × length) were cut from the plates arbitrarily. And the tensile specimens are cut 35 mm in width and 100 mm in gauge length.

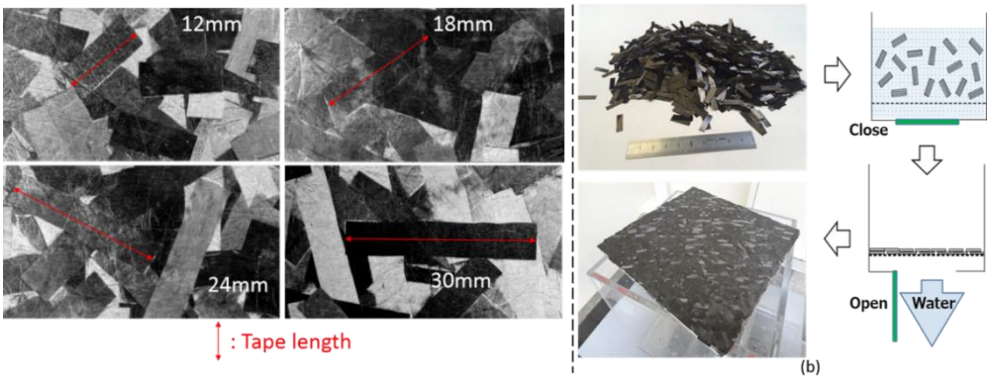

Figure 1: UT-CTT and the wet-type paper making process.

2.2 X-ray micro-CT analysis

The internal structural information of UT-CTT was observed and collected by the 3D X-ray scan system TDM1000-II from Yamato Scientific Co., Ltd. During the observation, the specimens were fixed on a rotational stage (Fig. 4), and the distance between the rotation axis and the radiation source is set to 10 mm for reliable resolution of embedded fibers on the images. The scanned volume is a right circular cylinder because of the rotation, and the size of the cylinder is 0.88 mm in radius and 1.76 mm in height. To ensure sufficient image resolution during CT acquisition process, the sample was positioned in the scanner's field of view so that the imaged volume had a physical size of 1×1×1 mm and excluded the air surrounding the sample. The X-ray tube voltage was set to 40 kV and X-ray tube current was set to 40 μA for all the specimens. After the acquisition of the X-ray projection images (a rotation step of 0.24 degree and 25 minutes per full rotation of the sample), the 3D image was reconstructed by the image processing unit of the X-ray CT system. The pixel size of the reconstructed 3D micro-CT images was fixed to 4 μm, and 512 images stacked through out-of-plane direction for each specimen were used for image processing and calculations. The schematic of scanning process and scanned volume are illustrated in Fig. 2.

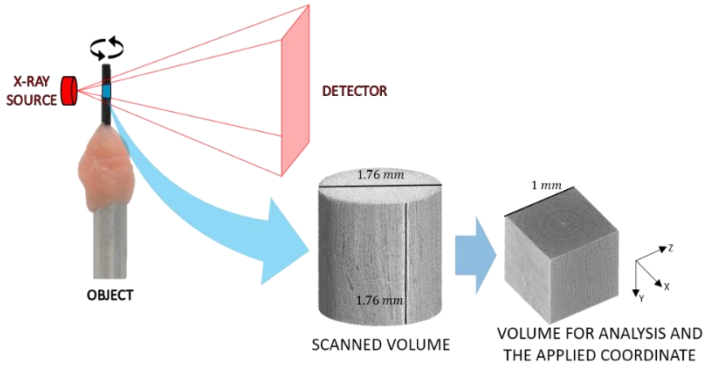

Figure 2: Schematic of scanning process and scanned volume of the UT-CTT [33].

Two different micro-CT methods are adopted in present study. One method is developed under the collaboration with KULeuven [33] and using a structural tensor based software named VoxTex. Another method is using a commercially available image binarization based software named TRI/3D-BON (RATOC System Engineering Co., Ltd.).

In the developed VoxTex method, CT images were converted from the native scanner format to a single three-dimensional array $I(X,Y,Z)$ of 8-bit grey values, where the coordinates X,Y,Z are integer numbers. The analyzed variables were the fiber orientation angles φ and θ in a spherical coordinate system: φ is the in-plane orientation angle, with the Cartesian axes X and Y lying in the plane of the sheet, and θ is the angle of a vector along the Z axis, normal to the X and Y axes. The fiber orientation vector is calculated from the CT image $I(X,Y,Z)$ using the three-dimensional grey value structure tensor [18, 33].

The histogram of FOD, averaged φ and θ through out-of-plane direction and orientation-quantified 3D model of UT-CTT were generated based on these two methods, and the orientation details are applied to the further mechanical modeling processes.

2.3 Tensile tests

Tensile experiments were conducted for UT-CTT. five specimens were prepared for all the UT-CTT with different tape lengths. The tensile stroke rate was set to 5 mm/min, the strains were measured using an extensometer, and the tensile strengths were measured as the maximum stress until final breaking occurred.

The tensile experiments of the matrix were also conducted to obtain the elastoplastic performances needed for the simulations. The dumbbell tensile specimens were manufactured by the corresponding resins, i.e., PA6, using injection molding processes. The tensile stroke rate was set to 1 *mm*/*min*. Because the fracture strains of these resins are much higher (higher than 30%) than that of the CF (about 2%) and the composites (less than 2%), only 5% strain of the matrices were recorded by the extensometer to ensure measurement accuracy. The stress–strain curves of the matrices are fitted based on the J_2-plasticity model, which is given by:

$$\sigma_{eq} = \begin{cases} \boldsymbol{C}:\epsilon^e & J_2(\sigma) \le \sigma_Y \\ \sigma_Y + kp + R_\infty[1 - e^{-mp}] & J_2(\sigma) > \sigma_Y \end{cases} \tag{1}$$

where $J_2(\sigma)$ is the von Mises equivalent stress; σ_{eq} and σ_Y denote the equivalent Cauchy stress and the yield stress, respectively; ϵ^e is the elastic strain; $\boldsymbol{C}$ is the Hooke's operator; and *k*, R_∞ and *m* denote the linear hardening modulus, hardening modulus, and hardening exponent, respectively. The parameter *p* represents the accumulated plastic strain and is expressed as:

$$p = \int \sqrt{\frac{2}{3} d\epsilon_{ij}^p d\epsilon_{ij}^p} \tag{2}$$

The J_2-plasticity model curve is plotted using the experimental data, and the parameters used in the fitting J_2-plasticity curves are applied to the simulation processes.

2.4 Mechanical property characterization

Two different modeling methods were applied in this study. The first one is the general analytical homogenization method for discontinuous inclusions: the modified Mori-Tanaka model [34]. The other one is the de-homogenization method well used on short fiber composites recently: the equivalent laminate method [24, 26].

The general Mori–Tanaka formulation to describe composites with randomly oriented inclusions was presented by Benveniste as follows [34]:

$$\boldsymbol{E}^{MT} = \boldsymbol{E}_m + V_f\{(\boldsymbol{E}_f - \boldsymbol{E}_m):\boldsymbol{T}\}:[V_m\boldsymbol{I} + V_f\{\boldsymbol{T}\}]^{-1} \tag{3}$$

where $\boldsymbol{E}$ denotes the stiffness tensor, and subscripts *m* and *f* represent the matrix and fiber, respectively. The curly bracket $\{.\}$ stands for orientation averaging. Tensor $\boldsymbol{T}$ is given by:

$$\boldsymbol{T} = [\boldsymbol{I} + \boldsymbol{S}_m:{\boldsymbol{E}_m}^{-1}:(\boldsymbol{E}_f - \boldsymbol{E}_m)]^{-1} \tag{4}$$

where $\boldsymbol{S}_m$ is Eshelby's tensor [28].

On the other hand, in the equivalent laminate method, the moduli of single equivalent layer, like E11 (aligned fiber direction), E22 (transverse to aligned direction), G12 (in-plane shear), and G13 (out-of-plane shear) are calculated by modified Mori-Tanaka model provided by Tandon and Weng [35, 36]:

$$\boldsymbol{E_{11}^{MT}} = \frac{\boldsymbol{E_m}}{\boldsymbol{1 + \frac{c(A_1 + 2\nu_m A_2)}{A}}} \tag{5}$$

$$\boldsymbol{E_{22}^{MT}} = \frac{\boldsymbol{E_m}}{\boldsymbol{1 + \frac{c}{2A}[-2\nu_m A_3 + (1-\nu_m)A_4 + (1+\nu_m)A_5 A]}} \tag{6}$$

$$\mathbf{G_{12}^{MT}} = \mathbf{G_m} + \frac{\mathbf{G_m c}}{\mathbf{\frac{G_m}{G_{p12} - G_m} + 2(1-c)S_{1212}}} \tag{7}$$

$$\boldsymbol{G_{13}^{MT}} = \boldsymbol{G_m} + \frac{\boldsymbol{G_m c}}{\boldsymbol{\frac{G_m}{G_{p13} - G_m} + 2(1-c)S_{1313}}} \tag{8}$$

where $\boldsymbol{A}$ and $\boldsymbol{A_i}$ are constants depending on the components of the Eshelby tensor and the matrix/fiber properties.

After the moduli of single equivalent layer are obtained, the mechanical properties of the equivalent laminate are calculated by the classical laminate theory (CLT). During the processes, the effect of defects are also considered. The fiber waviness is modeled by assuming the waviness to a sign wave and using the waviness amplitude of the sign wave as the parameter to calculate the effects [37].

In present study, the general Mori-Tanaka model simulation is running in the mean field modeling software Digimat-MF from e-Xstream engineering Co., while the equivalent laminate method is analyzed by the MCQ (Material Characterization and Qualification) chopped from AlphaStar Co.

3 RESULTS AND DISCUSSIONS

3.1 X-ray micro-CT analysis from VoxTex

In VoxTex processes, the distance between voxels for averaging calculation, which defines a volume for averaging, called below "volume of interest" (VOI), needs to be determined related to the thickness direction of the image UT-CTT during model constructions. The VOI's through-thickness dimension was set to 13 pixels, i.e., 44.2 µm to ensure that the thickness of each VOI is close to the thickness of a single tape (44 µm in average). Other two dimension of VOIs were equal to the extents of the image. The VOIs were numbered according to their order in position along the thickness direction: VOI 1 to VOI 25. All volumes of interest have a hexahedral shape.

After CT images were collected by the 3D X-ray scanner, the 3D models of UT-CTT were reconstructed (Fig. 2, right). The UT-CTT models exhibit layered structure, also the individual tapes in the UT-CTT show not-perfectly-flat orientations. In the next step, the visualized 3D model and histograms of fiber orientation distribution were constructed using the stacked micro-CT images (Fig. 3). The angles are given in the global Cartesian coordinate system (X, Y, Z) identical to the Cartesian system (x_1, x_2, x_3) introduced previously. The color in the sample of in-plane orientation visualized 3D models (Fig. 3 (a)) indicated local in-plane fiber orientation angle φ_{XY} (Phi_XY), with degree (°) as the unit. The sample of two-dimensional histogram combined in-plane (φ_{XY}, Phi_XY) and out-of-plane (θ_{XY}, Theta_XY) fiber orientation distribution angle is illustrated in Fig. 3 (b), where the color bar in this figure and also in Fig. 3 (c) and (d) indicate the data density. The orientation distribution shows the in-plane oriented feature of tapes imbedded in the samples. The orientation clusters are observed in the histogram, and to investigated this orientation concentration, the distributions of φ_{XY} and θ_{XY} were "unfolded" through the out-of-plane direction as shown in Fig. 3 (c) and Fig. 3 (d) respectively to analyze their change through the thickness. The unfolded φ_{XY} and θ_{XY} were calculated by each VOI, which means that the orientation distribution in each row in Fig. 3 (c) and Fig. 3 (d) shows the realistic tape orientation information in the corresponding layer position in the samples. The clusters observed in the unfolded φ_{XY} histogram indicate the fiber clusters with their corresponding orientation preferences, and this phenomenon exhibits the unique internal geometry properties of ROS that not observed in other discontinuous CFRP systems. The unfolded θ_{XY} histogram exhibits a concentrated distribution up to 90°. For more detail study

of the orientation distribution, the mean value and standard deviations (SD) of both φ_{XY} and θ_{XY} were also calculated by each VOI separately (Fig. 3 (e) and Fig. 3 (f)).

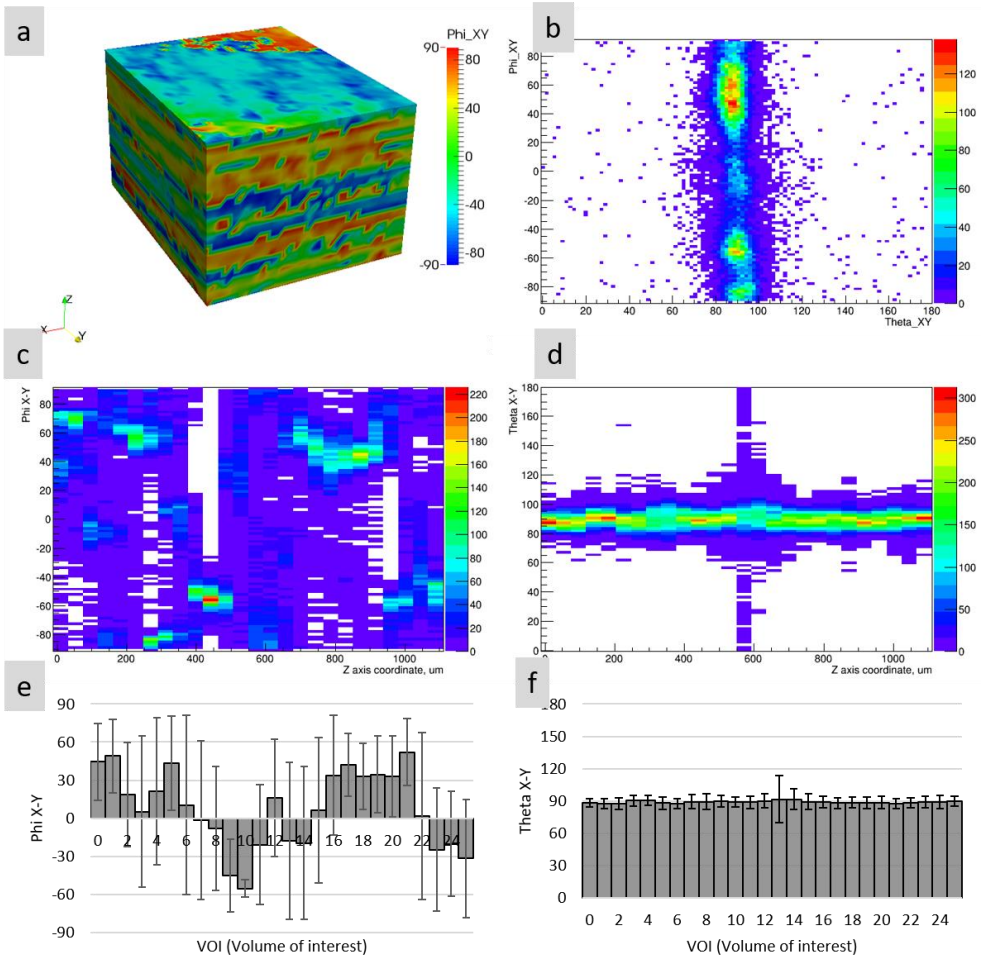

Figure 3: An example of VoxTex processing: visualized 3D model (a), orientation distribution (b), unfolded distributions of φ_{XY} (c) and θ_{XY} (d), and average values with standard deviations (SD) of φ_{XY} (e) and θ_{XY} (f) of UT-CTT.

To study the clusters of φ_{XY} in detail, the 3D model with φ_{XY} distribution (Fig. 3 (a)) is combined with the unfolded φ_{XY} histogram through z axis (Fig. 3 (c)) [33]. The subsets of the 3D model separated by the VOI were extracted following the clusters that appeared in the unfolded φ_{XY} histogram, which means that the 3D morphologies of the orientation concentration areas (the clusters in Fig. 3(c)) can be specified and extracted from the general 3D model (Fig. 3 (a)). The VOI 4 to 7, 9 to 11 and 16 to 21 are shown in Fig. 10. After the subsets were extracted, the threshold of φ_{XY} is applied on the model to identify the fiber distributions in concentrated φ_{XY} and the threshold ranges are also illustrated in Fig. 4. The extracted 3D models with threshold of φ_{XY} and the corresponding areas in unfolded φ_{XY} histogram proved the assumption that the tapes can interact during the wet process and disturb the ideal uniformly random orientation distribution, which would exist if the placements of the tapes were independent. The existence of the φ_{XY} distribution clusters through z axis is due to the tapes with the same orientation sticking together during the wet-type paper making process, as well as tape waviness and tape splitting taking place locally during the compression molding process. The 3D model of VOI 4 to 7 demonstrates 4 different layers (tapes) with the same orientation distribution pattern. In contrast, the 3D model of VOI 9 to 11 shows an integral part of tape with some scattered areas which are considered to be the tape waviness and splitting. On the other hand, the 3D models of VOI 16 to 21 exhibit both structural features: tapes are stuck together at the top of the model, while scattered areas

are observed on the bottom side. The combination of the 3D model with the unfolded φ_{XY} histogram shows a high capability for the quantitative internal geometry study of the UT-CTT with complex structural features. By extracting the subsets models, the detail structures and tape positions are reconstructed visually.

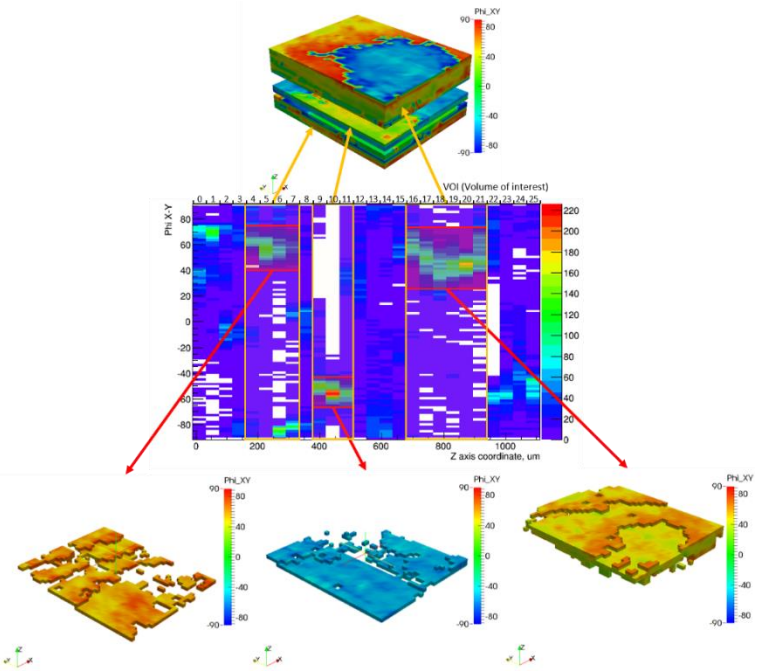

Figure 4: Unfolded φ_{XY} histogram and the corresponding clusters in visualized 3D model.

3.2 X-ray micro-CT analysis from 3D-BON

On the other hand, the 3D X-ray micro-CT analysis using 3D-BON show some difference in the results. The in-plane and out-of-plane orientation distribution and visualized meso-structure model of UT-CTT were built by this software. Also, the orientation tensors of UT-CTT were calculated based on the average in-plane and out-of-plane angle summarized by this software. The equation for orientation tensor calculation is:

$$\boldsymbol{O} = \begin{bmatrix} \cos^2\phi \sin^2\theta & \sin\phi\cos\phi\sin^2\theta & \cos\phi\sin\theta\cos\theta \\ \sin\phi\cos\phi\sin^2\theta & \sin^2\phi\sin^2\theta & \sin\phi\sin\theta\cos\theta \\ \cos\phi\sin\theta\cos\theta & \sin\phi\sin\theta\cos\theta & \cos^2\theta \end{bmatrix} \tag{9}$$

where $\boldsymbol{O}$ denotes the fiber orientation, ϕ is the average in-plane angle and θ is the average out-of-plane angle of the materials.

The basic algorithm of 3D-BON based on the general image binarization process and the fiber monofilaments are separated from the X-ray images and rebuild 3D model under the resolution of single fibers (Fig. 5). In this figure, fiber monofilaments can be observed easily.

In the next step, the image binarization process was running for the calculation and modeling of both in-plane and out-of-plane orientation properties of the meso-structure. The 3D model with the in-plane orientation information and out-of-plane information are illustrated in Fig. 6. Studying the figures, the fibers show good aligned in-plane orientation through thickness direction, which is the orientation feature of ROS that the structure has locally laminated property. In addition, the out-of-plane orientation indicated that most of the fibers are lie down in the in-plane direction, but there are still some fibers oriented through out-of-plane direction show blue and yellow colors in Fig. 6 (b).

The orientation tensors of UT-CTT were calculated based on the average orientation angles collected from this method and will be inputted to the simulation process as the realistic orientation information of UT-CTT to obtain better simulation accuracy.

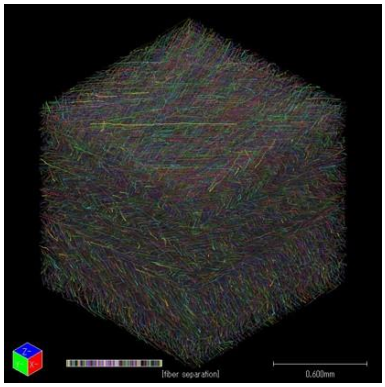

Figure 5: 3D model build by TRI/3D-BON method under fiber level resolution [38].

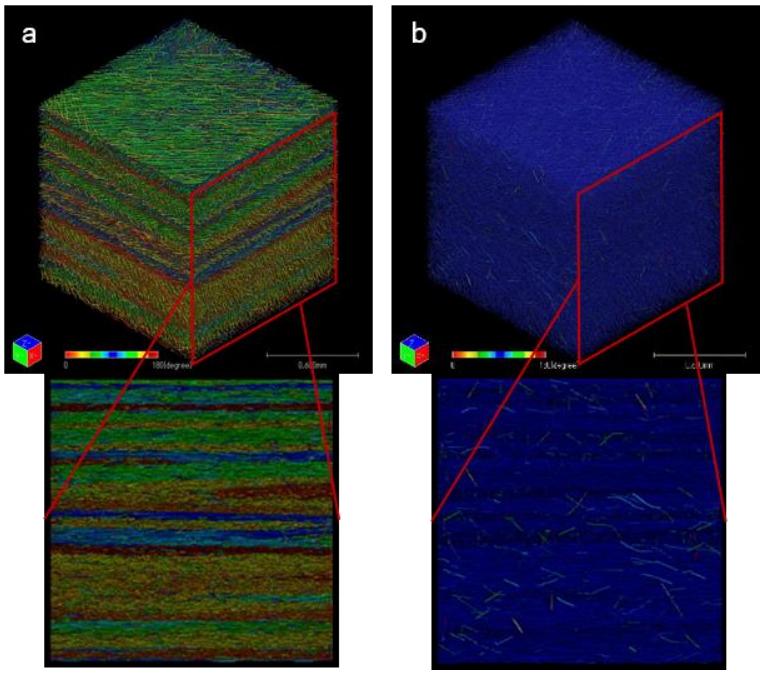

Figure 6: The 3D structural model with φ_{XY} and θ_{XY} distribution of UT-CTT (the color bar indicates the orientation angle from 0 to 180 degree) [38].

3.3 Modeling and simulation of UT-CTT

The V_f of UT-CTT in different tape lengths calculated by the ash test as well as the equivalent aspect ratio of the tapes [39] are presented in Table 1. The V_f show subtle difference between each tape length and is regarding caused by the complex interactions during molding processes. The table 1. also indicate the equivalent aspect ratio of the tape is much lower than the aspect ratio of single fiber with same length. Lower aspect ratio will lead to lower mechanical properties in simulation, which support the fact that the multi-scale interphase can generate structural defects in UT-CTT. The mechanical properties of the constituent properties at the fiber and matrix scales are listed in Table 2. and Table 3., respectively [40].

Tape length (mm)	12	18	24	30
Fiber V_f (%)	52.2	55.1	52.8	53.1
Aspect ratio	212	305	400	497

Table 1: V_f of UT-CTT in different tape lengths.

	Young's Modulus E (GPa)	Tensile Strength σ (MPa)	Fracture Strain ε_f (%)	Diameter d (μm)	Density ρ (g/cm^2)
TR 50	240	4900	2.0	7	1.82

Table 2: Mechanical properties of the carbon fiber used in this study.

	Density ρ(g/cm^2)	Poisson's Ratio v	Young's Modulus E (GPa)	Yield Stress σ_Y (MPa)	Hardening Modulus R_∞ (MPa)	Hardening Exponent m	Linear Hardening Modulus k (MPa)	Equivalent matrix tensile strength σ_m^* (MPa)
PA6	1.14	0.40	3.31	15.0	56	350	160	55

Table 3: Mechanical properties of the matrix used in this study.

Input the measured data into both the general Mori-Tanaka model and the equivalent laminate model, the simulation results were compared with the experimental tensile results both on moduli and strengths, and the results are illustrated in Fig. 7. The experimental results of UT-CTT show high tensile preference compare with general discontinuous CFRTP. Also, an increasing tendency can be clearly observed in tensile strengths, while although changed can be found in the moduli, but the change of V_f will weaken the change derived from tape length.

The Mori-Tanaka and equivalent laminate simulation both show considerable results comparing with the experimental values. On the other hand, these two methods also show difference in prediction accuracy:

The general Mori-Tanaka model match very good with the experimental values in moduli, the results also predicted the change lead by the change of V_f. While the moduli in equivalent laminate method are higher than the experimental values in all the tape lengths. This result indicate that in prediction of the elastic properties, Mori-Tanaka model can do better job on ROS, and the equivalent laminate method still overestimate the moduli because the method considered the ROS as continuous laminate and the defects as waviness have less effect on the elastic properties.

On the other hand, the Mori-Tanaka model cannot simulate the change of strength caused by the change of tape length but the equivalent laminate method can predict the increasing tendency of strength to tape length considerably. The reason for this difference is mainly based on the capability of structural properties definition. In Mori-Tanaka model, only the simple fiber orientation distribution has been considered, while the equivalent laminate method not only counted the fiber orientation but also considered the defect effects of fiber waviness. Because the internal geometry irregularities have great effect on the fracture propagation of CFRTP, so the equivalent laminate method show better matching with the experimental results.

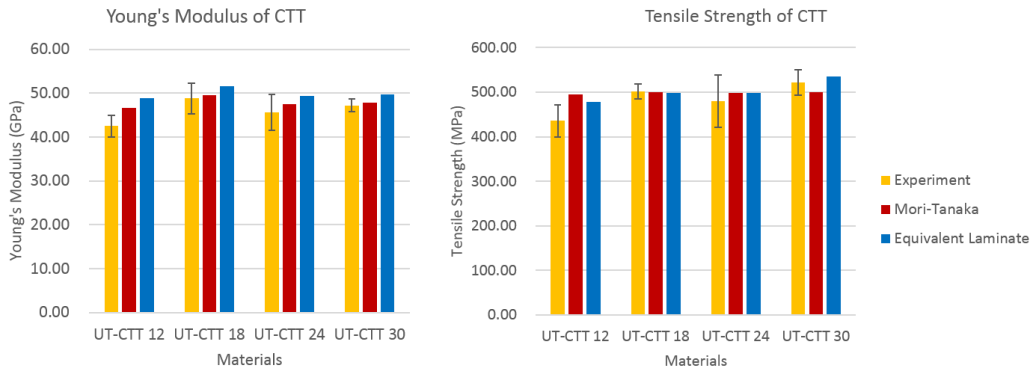

Figure 7: Comparison of tensile properties between experimental results and simulation results.

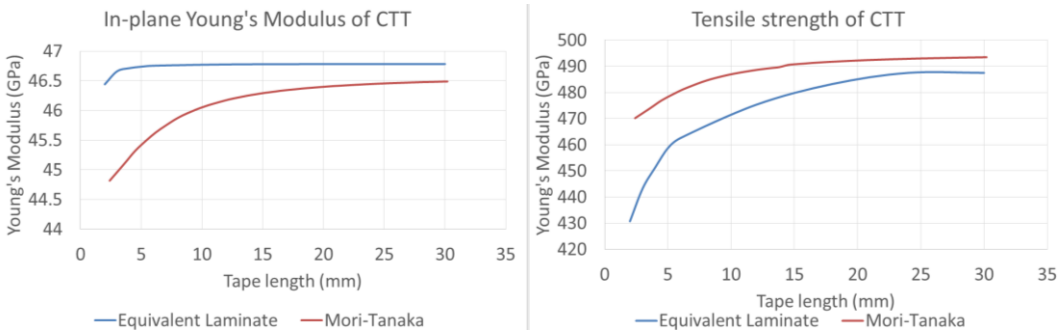

Figure 8: Tape length dependency simulations of UT-CTT.

Because both these two models exhibit their simulation capabilities in different aspects, the results open a new door for the simulation of UT-CTT for material characterization and industrial applications. For instance, because the tape length shows important effects on the mechanical properties of UT-CTT, so the application of this material need consider the required mechanical properties and corresponding tape length to ensure the application efficiency. Based on the two models introduced in this study, the tape length dependency of UT-CTT is simulated as shown in Fig. 8. For simplicity, the fiber V_f is set to 50% and the fiber orientation is considered as 2D random (with waviness 5° for equivalent laminate model). Also the tape thickness is fixed to 50 μm together with 5 mm tape width. The simulation result also indicated the difference in prediction accuracy as discussed, and this result can be provided as a material indicator for the corresponding applications.

4 CONCLUSIONS

In present study, two different X-ray micro-CT methods and two simulation models are applied for the internal geometry analysis and mechanical property characterization of UT-CTT, an ROS-structured CFRTP.

The applied X-ray micro-CT methods analyzed FOD, tape waviness, and splitting of the internal geometry of UT-CTT from different aspects. The VoxTex provided detailed layer-based orientation distribution, and the tape morphologies after molding are visualized. On the other hand, the 3D-BON calculated fiber monofilaments FOD, and the averaged fiber orientation tensors are calculated under denser φ_{XY} and θ_{XY} distribution data.

The modeling of UT-CTT are conducted with the consideration of the acquired internal geometry results. In the general Mori-Tanaka model, the orientation tensors calculated from 3D-BON are used; in the equivalent laminate model, the out-of-plane waviness is quantified based on the θ_{XY} distribution results from VoxTex. The simulation results show considerable matching with the tensile experiment data. The comparison indicated the Mori-Tanaka model have better simulation accuracy in tensile moduli and the equivalent laminate model can reproduce the strength-tape length relationship thanks for the consideration of structural irregularity. Finally, the tape length dependency of UT-CTT is simulated using the methods introduced in this study, and the result can be provided as a material indicator for the corresponding industrial applications.

ACKNOWLEDGEMENTS

This study was supported in part by a Research Fellowship of the Japan Society for the Promotion of Science, Grant-in-Aid for JSPS Research Fellow Grant Number JP15J09248.

Part of this study was conducted as Japanese METI project "the Future Pioneering Projects / Innovative Structural Materials Project" since 2013 financial year. Authors would like to express sincerely appreciation to the project members who have provided valuable information and useful discussions.

REFERENCES

[1] S. Sihn, R. Y. Kim, K. Kawabe, et al. Experimental studies of thin-ply laminated composites. Compos Sci Technol. 2007;67(6):996-1008.
[2] T. Yokozeki, Y. Aoki, T. Ogasawara. Experimental characterization of strength and damage resistance properties of thin-ply carbon fiber/toughened epoxy laminates. Compos Struct. 2008;82(3):382-389.
[3] R. Amacher, J. Cugnoni, J. Botsis, et al. Thin ply composites: Experimental characterization and modeling of size-effects. Compos Sci Technol. 2014;101:121-132.
[4] P. Feraboli, T. Cleveland, M. Ciccu, et al. Defect and damage analysis of advanced discontinuous carbon/epoxy composite materials. Compos Part a-Appl S. 2010;41(7):888-901.
[5] M. Selezneva, L. Lessard. Characterization of mechanical properties of randomly oriented strand thermoplastic composites. J Compos Mater. 2016;50(20):2833-2851.
[6] B. Landry, P. Hubert. Experimental study of defect formation during processing of randomly-oriented strand carbon/PEEK composites. Composites Part A: Applied Science and Manufacturing. 2015;77:301-309.
[7] J. Takahashi. Expectations and challenge of thermoplastic CFRP. SAMPE Japan symposium "Future of automobile pioneered by advanced materials", Tokyo, Japan. 2016.
[8] A. Alemdar, H. Zhang, M. Sain, et al. Determination of fiber size distributions of injection moulded polypropylene/natural fibers using X-ray microtomography. Adv Eng Mater. 2008;10(1-2):126-130.
[9] A. Bernasconi, F. Cosmi, D. Dreossi. Local anisotropy analysis of injection moulded fibre reinforced polymer composites. Compos Sci Technol. 2008;68(12):2574-2581.
[10] A. Bernasconi, F. Cosmi, P. J. Hine. Analysis of fibre orientation distribution in short fibre reinforced polymers: A comparison between optical and tomographic methods. Compos Sci Technol. 2012;72(16):2002-2008.
[11] Y. Abdin, S. V. Lomov, A. Jain, et al. Geometrical characterization and micro-structural modeling of short steel fiber composites. Compos Part a-Appl S. 2014;67:171-180.
[12] T. B. Nguyen Thi, M. Morioka, A. Yokoyama, et al. Measurement of fiber orientation distribution in injection-molded short-glass-fiber composites using X-ray computed tomography. J Mater Process Tech. 2015;219:1-9.
[13] X. Sun, J. Lasecki, D. Zeng, et al. Measurement and quantitative analysis of fiber orientation distribution in long fiber reinforced part by injection molding. Polymer Testing. 2015;42:168-174.
[14] G. Requena, G. Fiedler, B. Seiser, et al. 3D-Quantification of the distribution of continuous fibres in unidirectionally reinforced composites. Composites Part A: Applied Science and Manufacturing. 2009;40(2):152-163.
[15] S. Dietrich, J. M. Gebert, G. Stasiuk, et al. Microstructure characterization of CVI-densified carbon/carbon composites with various fiber distributions. Compos Sci Technol. 2012;72(15):1892-1900.
[16] K. I. Tserpes, A. G. Stamopoulos, S. G. Pantelakis. A numerical methodology for simulating the mechanical behavior of CFRP laminates containing pores using X-ray computed tomography data. Composites Part B: Engineering. 2016;102:122-133.
[17] M. Barburski, I. Straumit, X. W. Zhang, et al. Micro-CT analysis of internal structure of sheared textile composite reinforcement. Compos Part a-Appl S. 2015;73:45-54.
[18] I. Straumit, S. V. Lomov, M. Wevers. Quantification of the internal structure and automatic generation of voxel models of textile composites from X-ray computed tomography data. Composites Part A: Applied Science and Manufacturing. 2015;69:150-158.
[19] N. Naouar, E. Vidal-Salle, J. Schneider, et al. 3D composite reinforcement meso F.E. analyses based on X-ray computed tomography. Compos Struct. 2015;132:1094-1104.
[20] G. W. Melenka, E. Lepp, B. K. O. Cheung, et al. Micro-computed tomography analysis of tubular braided composites. Compos Struct. 2015;131:384-396.
[21] S.-Y. Fu, B. Lauke. Effects of fiber length and fiber orientation distributions on the tensile strength of SFRP. Compos Sci Technol. 1996;56:12.
[22] S. Y. Fu, B. Lauke, E. Mader, et al. Tensile properties of short-glass-fiber- and short-carbon-fiber-reinforced polypropylene composites. Compos Part a-Appl S. 2000;31(10):1117-1125.

[23] M. R. Piggott, M. Ko, H. Y. Chuang. Aligned Short-Fiber-Reinforced Thermosets - Experiments And Analysis Lend Little Support for Established Theory. Compos Sci Technol. 1993;48(1-4):291-299.
[24] M. Hashimoto, T. Okabe, T. Sasayama, et al. Prediction of tensile strength of discontinuous carbon fiber/polypropylene composite with fiber orientation distribution. Compos Part a-Appl S. 2012;43(10):1791-1799.
[25] H. Moussaddy, D. Therriault, M. Levesque. Modeling elastic properties of randomly oriented fiber composites. ICCM 19, Canada2013.
[26] Y. Li, S. Pimenta. Analytical prediction of strength for tow-based discontinuous composites. 5th ECCOMAS Thematic Conference on Mechanical Response of Composites, Bristol, UK2015. p. 7–9.
[27] K. Tanaka, T. Mori. The hardening of crystals by non-deforming particles and fibres. Acta Metallurgica. 1970;18(8):931-941.
[28] J. D. Eshelby. The Determination of the Elastic Field of an Ellipsoidal Inclusion, and Related Problems1957.
[29] N. Bn, J. Paquette. EMTA's Evaluation of the Elastic Properties for Fiber Polymer Composites Potentially Used in Hydropower Systems. Richland, WA, U.S.: Pacific Northwest National Laboratory; 2010.
[30] J. Schjodt-Thomsen, R. Pyrz. The Mori-Tanaka stiffness tensor: diagonal symmetry, complex fibre orientations and non-dilute volume fractions. Mech Mater. 2001;33(10):531-544.
[31] B. N. Nguyen, S. K. Bapanapalli, V. Kunc, et al. Prediction of the Elastic-Plastic Stress/Strain Response for Injection-Molded Long-Fiber Thermoplastics. J Compos Mater. 2009;43(3):217-246.
[32] Y. Wan, J. Takahashi. Tensile and compressive properties of chopped carbon fiber tapes reinforced thermoplastics with different fiber lengths and molding pressures. Composites Part A: Applied Science and Manufacturing. 2016;87:271-281.
[33] Y. Wan, I. Straumit, J. Takahashi, et al. Micro-CT analysis of internal geometry of chopped carbon fiber tapes reinforced thermoplastics. Composites Part A: Applied Science and Manufacturing. 2016;91, Part 1:211-221.
[34] Y. Benveniste. A new approach to the application of mori-tanaka theory in composite-materials. Mech Mater. 1987;6(2):147-157.
[35] G. P. Tandon, G. J. Weng. The Effect Of Aspect Ratio Of Inclusions on the Elastic Properties Of Unidirectionally Aligned Composites. Polym Composite. 1984;5(4):327-333.
[36] S. Dormohammadi, F. Abdi, R. Mandapati, et al. Impact Crush Modeling of Chopped Fiber Reinforced Polymers. American Society for Composites 30th Technical Conference, Kellogg Center, Michigan State University, East Lansing, Michigan, U. S.2015. p. 1899.
[37] D. L. Shi, X. Q. Feng, Y. G. Y. Huang, et al. The effect of nanotube waviness and agglomeration on the elastic property of carbon nanotube-reinforced composites. J Eng Mater-T Asme. 2004;126(3):250-257.
[38] Y. Wan, J. Takahashi. Meso-structural quantification and visualization of ROS of thermoplastic composites. 8th Japan Conference on Composite Materials, Tokyo, Japan2017.
[39] Y. Wan, J. Takahashi. Tensile properties and aspect ratio simulation of transversely isotropic discontinuous carbon fiber reinforced thermoplastics. Compos Sci Technol. 2016;137:167-176.
[40] Y. Wan, J. Takahashi. CFRTP mechanical properties simulation by Mori-Tanaka model and equivalent laminate methods. 17th European Conference on Composite Materials, Munich, Germany2016.